IOWA STATE UNIVERSITY
Digital Repository

2011

Characteristics of dielectric elastomers and fabrication of dielectric elastomer actuators for artificial muscle applications

William Lai
Iowa State University

Follow this and additional works at: https://lib.dr.iastate.edu/etd

Part of the Aerospace Engineering Commons

Characteristics of dielectric elastomers and fabrication of dielectric elastomer actuators for

artificial muscle applications

by

William Lai

A thesis submitted to the graduate faculty

in partial fulfillment of the requirements for the degree of

MASTER OF SCIENCE

Major: Engineering Mechanics

Program of Study Committee:

Ashraf Bastawrows, co-Major Professor

Wei Hong, co-Major Professor

Thomas J Rudolphi

Iowa State University

Ames, Iowa

2011

Table of Contents

List of Figures

Abstract

Electroactive polymers have been studied for artificial muscle applications in last decades. One of the EAP materials, 3M VHB acrylic tapes, have shown been outstanding electro-mechanical coupling performance. The scope of this study is to understand the electro-mechanical properties of VHB acrylic material. In addition, the research explores new practical designs of soft actuators. The basic designs employ directional planar stiffeners that act as geometric constraints. The utilization of these stiffeners provides the ability to tailor the planar deformation into many three dimensional deformed shapes.

In the first part of this work, the material nonlinear mechanical response is characterized using a pre-stretched planar configuration with different bi-axial stretch ratios. Also, unequal bi-axial stretch ratios were also investigated. During the course of deformation, high resolution images of the deformed state were in situ captured. The images were analyzed by digital image correlation technique to evaluate the in-plane finite strain components. The measurements are used to calibrate a Neo-Hookean based material model that couples the applied electrical field to the actuator mechanical deformation. The material model is built into a user-material subroutine with the ABAQUS commercial finite element package. The numerical model is used to optimize different geometrical feature, electrode layup and stacking sequence for the actuator in order to attain a prescribed deformation pattern. The developed framework will aid in designing and optimizing the EAPs actuator configurations for general 3D prescribed deformation configuration.

In the second part of our work, we presented a new actuator design featuring a freestanding configuration without the constraints of pre-stretch. By using different configuration of stiffener reinforcement, the proposed design presented various complex three dimensional

motions. A simple one-dimensional planar stiffener is utilized to measure the resulting curvature of the deformed configuration under different level of applied voltage. The Timoshenko-bimaterial laminate solution is employed to assess the electrical to mechanical conversion efficiency. The developed framework will address more complex 3-D deformation. The whole work is a first step towards the development of soft actuators for artificial muscle applications.

Chapter 1. Introduction

1.1 Motivation

For last decades, biomimic actuators performing as artificial muscles have drawn much attention for compliant and lightweight robotic arms and grippers for tight spaces as well as energy-efficient actuators for biomimetic locomotion and flying [2]. In Mother Nature, we are inspired by octopus arm as example (see Fig. 1a), which can generate considerably large deformation with very high degree-of-freedom The attractive features of octopus arm come from its very complicated muscle structure that various different types of soft muscle cooperate together to generate movement without skeleton (Fig. 1b and c). Our goal is to develop soft actuators that are able to present such a complex mechanism. Thus, we look to start from fundamental study of materials and structures for unit-cell of soft actuators which are the foundation of developing future artificial muscles applications.
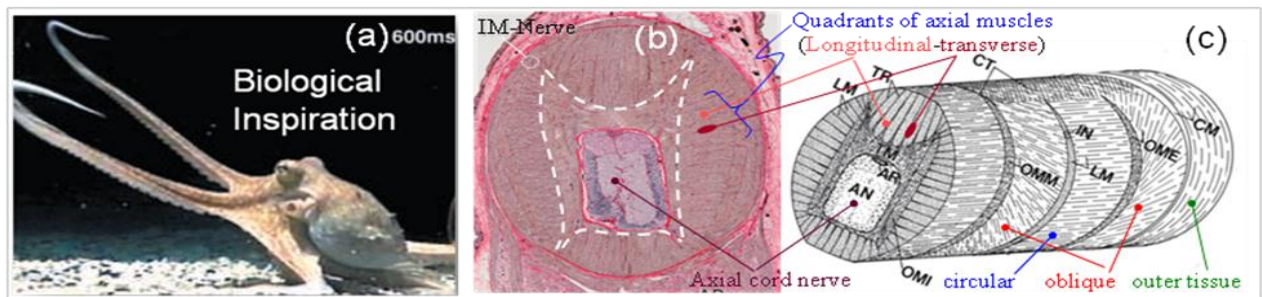
Fig. 1 Muscle structure of octopus arms. [33] [34]

1.2 Overview

To develop a practical biomimic actuator with good performance, our first objective is to establish a practical framework. At the very beginning of framework development, it is of great

importance to choose a suitable material. From literatures, we have noticed dielectric elastomers, a group of electroactive polymers (EAPs), have especially been considered for artificial muscle application due to their high strain, comparably short response time, low cost, and high electromechanical coupling efficiency [12] [21] [23] [26]. Basically, electric elastomer actuators (DEAs) are made of incompressible soft dielectric elastomer membranes sandwiched between compliant electrode layers to form dynamic capacitors. When electric field is applied across the electrodes, the columbic force generates a stress called Maxwell stress [25] that attracts other electrodes together and squeezes the sandwiched dielectric elastomer layer. As a result, the in-plane expansion of DEA can be observed due to elastomer incompressibility. From many different DE materials, we choose 3M VHB acrylic as the major materials in our study because of their outstanding performance [7] as well as the availability which make them very good for prototyping new concept of actuators.

Next step, we are focusing on the characteristic of the material. To study material properties through experiments, we fabricate samples with different ratio of biaxial prestretch induced on the horizontal and vertical direction. After applying electric field, actuation strain field can be measured and investigated for material characterization. For measurement, we capture planar actuation through high resolution CCD camera in a situ imaging system and analyze images by using digital image correlation method. The experiments are carried out for calibration of the framework we developed that coupling the applied electric field to the actuator mechanical deformation. The material model used in the framework was Neo-Hookean based and built into a user-material subroutine with the ABAQUS commercial finite element package provided by Dr. Wei Hong. The framework will aid in designing and optimizing the EAPs actuator configurations for general 3D prescribed deformation configuration.

The second part of our work is focusing on a new concept of fabricating DEAs. We present a new design for a dielectric elastomer actuator (DEA) with geometrically confining reinforcement. The resulting structures enable complex 3-dimentional motions without the need of the DEA prestretch and the support of hard frame. An in situ imaging system is used to capture the complex deformation pattern to evaluate the surface curvatures. The deformation mode is analyzed analytically using the bi-laminate theory to develop a closed form representation amenable for control strategies. The finite element material model developed in the first part of our work is used to analysis the more complex deformation patterns. The proposed confining reinforcement strips would enable the development of flexible continuous robotics, utilizing combination of the proposed deformation mechanisms to provide controllable many degrees of freedom.

Chapter 2. Literature Review

2.1 Material Background

To develop actuators for artificial muscle applications, we are looking for "smart materials" (which may deform by triggered through certain stimulations) with muscle-like features which including light, soft, and short responding time [2]. In literatures, we have seen numerous smart materials being proposed; however, each of them has its benefits and limitations in applications of artificial muscle. For example, piezoelectrics work nicely under high frequency situation, but their low strain and high stiffness are not suitable for muscle application [2] [17]. On the other hand, shape memory alloys are able to have large strain but suffering from time consumption of cooling alloy in order to recover [10]. Fortunately, there is a group of smart polymers, electroactive polymers (EAPs), proposed for the most suitable candidates of artificial muscle applications. Their human-muscle like features which are light, soft and can generate considerable large displacement with acceptable response time [2] [12] [17] have drawn much attention for soft actuators study.

As the name shows, EAPs are polymers capable of inducing deformation under electrical stimulation. Recently, there are several EAPs being widely studied. Based on mechanisms of actuation, they can broadly be divided into two categories: ionic EAPs, including Ionic polymer-metal composites (IPMCs) and conductive polymers (CPs), and field-activated EAPs, including ferroelectric polymers and dielectric elastomers (DEs) [12]. The method of Ionic EAPs is based on migration of ions triggered by applied electric force. General speaking, they have lower requirement of operating voltage around 10 volts but suffer from low frequency [12] and low energy efficiency [2]. On the other side, the method of field-activated EAPs is directly using electric force that they are theoretically having higher electromechanical coupling efficiency[12] .

In addition, they usually have larger strain response and relatively shorter response time [17]. However, much higher voltage is needed [2] [12] [25] for them to be actuated. Followings are brief introductions of these four different EAPs.

A. Ionic polymer-metal composites (IPMCs)

Ionic polymer-metal composites (IPMCs) have almost been studied in the past 20 years, which were initially proposed by Oguro et al. [13]. Theoretically, they are constructed with an ion-exchange polymer membrane sandwiched by two thin flexible metal (typically platinum or gold) electrode layers. This particular ion-exchange polymer, for example, 3M Nafion® 117, only allows the migration of cations. Therefore, while applying voltage (normally lower than 10 volts), mobile ions in the polymer membrane will flow toward anode of the IPMC (another explanation is that cations drag water molecular with them) and cause non-uniformed volume distribution which results in bending (with strain around 3%[12]) of the sample (see Fig. 2).
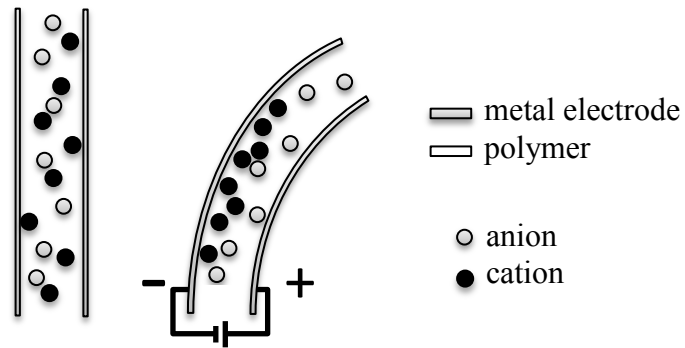
Fig. 2 Sketch of IPMC mechanism. When applying voltage, mobile ions, cations, in the polymer membrane will flow toward anode of the IPMC

B. Conductive polymers (CPs)

Conductive polymers (CPs) were first presented by Baughman et al. in 1990 [22]. The actuation of CPs based on interactions between polymer chains and solvent under

electrochemical redox reaction. During reduction, polymer chains will be attached by cations in the solvent and expands. In contrary, polymer chains will release the attached cations back to solvent and shrink during oxidation. Thus, the idea of CPs actuators is attaching two layers of CP connecting to opposite signs of electrodes, which could induce bending actuation (see Fig. 3). Although actuation voltages of CPs are low (1-2 volts [12]), the operating efficiency is unfortunately also low (~1% [12]).
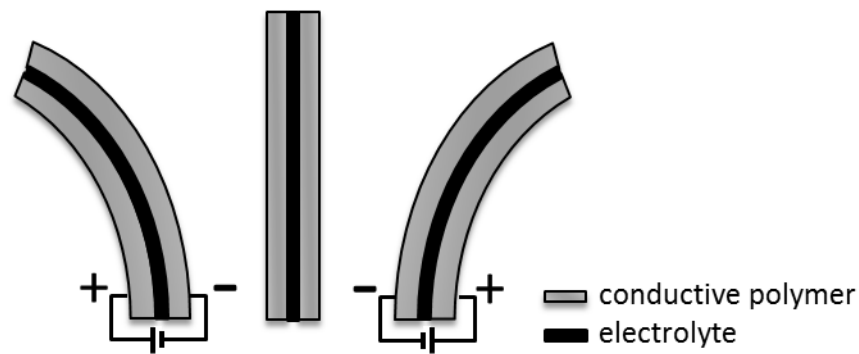
Fig. 3 Actuation mechanism of CPs

C. Ferroelectric polymers

Ferroelectric polymers are considered as analogous to ferromagnets, where the application of an electric field aligns polarized domains in the materials [17]. Since it's been observed that the permanent polarization exists even after the field is removed, the deformation of ferroelectric polymers is able to remain without continuously electro field applied. Ferroelectric EAPs can be operated in air, a vacuum, or water in a wide range of temperatures typically between 20 and 80 °C [17]. Poly (vinylidene fluoride-trifluoroethylene) (P(VDF-TrFE)) is a commonly used ferroelectric polymer which has a strain observation up to 7% and an elastic energy density above 1 MJ/m3 under an electric field of 150MV/m and a strain as high as 2% under a low applied field about 13 MV [12].

D. Dielectric elastomers (DEs)

Dielectric elastomer actuators (DEAs) have drawn a great attention since R. Pelrine et al. published their work in 1999 [32]. DEAs are made of an incompressible soft dielectric elastomer membrane with a layer of compliant electrode deposited on each side. When an electric field is applied across the plates working as a capacitor, the columbic force generates a stress called Maxwell stress [25] that results in attracting both plates together, squeezing dielectric elastomer membrane, and inducing expansion of DEA due to incompressibility of the elastomer (see Fig. 4). Typically, silicone or acrylics are used as dielectric elastomers, and carbon or graphite powder/grease or other highly compliant metal paints [12] are used as electrodes. Beside this, a process named prestretch is of great importance to DEAs. Prestretch means stretching thin films first and keeping them stretched before building actuators. It has been shown prestretch is able to effectively improve the performance of DEAs. The operating voltage of DEAs is high (~1-10 kV) [12] [17] which is around 100 MV/m of electric field. However, considerably high actuation strain (over 100%) [20] can be reached in the meantime.

One of the other benefits of DEs is the material availability. Several commercialized products have suggested in literatures [3] [5] [16] such as Dow Corning HS3 silicone [14], NuSil CF19-218 silicone [14], BJB Enterprice TC-5005 A/B-C silicone [4], and 3M VHB 4910 acrylic tapes [7] [8] [14] [21]. Among these easy-accessible commercial products, 3M VHB 4910 acrylic tapes show an impressive performance due to the high dielectric constant (4.7) [7] and high actuation strain potential that they are able to bare over 6 times of axial stretch on both planar directions [6]. In addition, with adhesive layer coated on surface, electrodes can be deposited on samples with no difficulty. This ease of manipulation is very suitable for prototype

assembly of different flexible actuator configurations. Therefore, VHB tapes are chosen be the major material in our study.
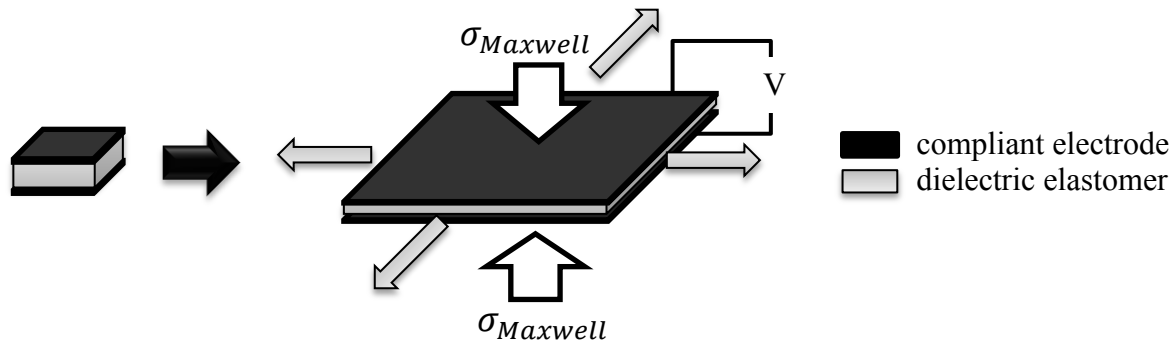
Fig. 4 Sketch of DEA. Sandwich structure of 2 compliant electrode layers and a dielectric elastomer membrane. When an electric field is applied, Maxwell stress will induce in-plane expansion due to incompressibility of dielectric elastomer membrane.

2.2 Review of Actuator Designs

Present, many configurations of DEAs have been studied and are mostly based on using large in-plane expansion for planar actuators. In addition, actuator designed by using thickness change of DEAs is also a common application. Besides, special structures with methods that can practically utilize energy stored from prestretch process have also been studied.

With no doubt, DEAs present notable planar strain; however, it is not the most suitable motion for biomimic devices and artificial muscle applications. Movements of muscle are often involving linear elongation or high-degree-of-freedom out-of-plane shape change. Besides, due to prestretch process, the necessity of fixing DEs membrane on firm frames causes a difficulty of building freestanding actuators. Accordingly, how to convert the basic area-expansion of DEAs into usable actuation with expected action and how to design freestanding structure have been the importance issues of developing DEAs for artificial muscle applications.

A robotic-arm design that S. Dubowsky et al. published in 2006 [1] showed some solutions. The configuration of each single unit transfers planar expansion into linear elongation by using a linear bistable element that enables only one direction of expansion. Linear bistable elements have two stable states that whole structure will be triggered into elongated state whenever expansion generates certain level of force. In addition, this structure is a semi-freestanding actuation that frame-included movement is presented instead of in-frame-only displacement.

Similarly, by combing DEAs with mechanical structures, P. Lochmatter et al. [18] presented a shell bending actuator with a stack of segments. Basically it a shell like structure with two planar actuators on top and bottom surfaces and a joint mechanical device in between. Bending can be observed once one side of DEAs is stimulated and expanded.

Stacking DEAs are the other approach of design that has been studied. The idea is to enlarge the thickness change of DEAs by stacking them up for axial shrinking actuators. G. Kovacs et al. published a design of cylindrical bar made of multi-layer of 3M VHB tapes with each layer separated by compliant electrodes [9]. Electrode layers were connected to outer voltage supply with alternating positive and negative signs. A maximum 30% of linear length reduction was shown after applying voltage in experiments. Also, a result of 1 kg mass lifting by 10% of contraction was also been observed. In addition, F. Carpi et al. also published two different methods, folding and helical, for manufacturing stacking actuators [4]. Both of them demonstrated more convenient fabricating process stacking DEAs.

Besides, different configurations of constructing DEAs by using unit planar actuators have also been proposed to have exciting results. For example, it has been shown that stacking planar expanding actuator and inactive layer together can induce bending and non-planar

movement [14]. Also, by rolling planar DEAs up, we may obtain an actuator with stroking motion perpendicular to rolling direction [14].

In addition, G. Kofod et al. brought up a fresh new idea called self-organized minimum-energy structures [8], which effectively use the stored energy generated by prestretch. Similar to tape measure, these special structures have two stable states. During relaxation, they curve for seeking minimum-energy state. After stimulated by applying a voltage, they stretch and become planar state. Considerable output force may also be produced in this design. They proposed these planar structures having several different 3-dimensional complex motions by fabricating them with different frame configurations.

Chapter 3. Development of Framework

3.1 General Introduction

To develop a practical biomimic actuator with good performance, establishing a practical framework can be very helpful for studying complex structures, and characterizing materials is the first step of framework establishment. The dielectric elastomers we choose for this study, 3M VHB acrylic tapes, have been shown the outstanding performance with excellent availability. From G. Kofod's and G. Kovas's previous work [6] [35], we understand that VHB is considered as hyperelastic material with nonlinear stress-strain relation. Besides, we also understand the performance of DEAs may have great improvement by introducing prestretch [6]. Based on these, we want to establish a practical framework that can present the electromechanical coupling of dielectric elastomers with considering the effect of prestretch.

The framework we use is a user-material subroutine with commercial finite element package, ABAQUS. This numerical model couples the applied electric field to the actuator mechanical deformation and is used to optimize different geometrical feature, electrode layup and stacking sequence for the actuator in order to attain a prescribed deformation pattern. A series of experiments of characterizing electromechanical response are running for framework calibration. We use a pre-stretched planar configuration with different biaxial stretch ratios as well as unequal biaxial stretch ratios for investigation. For measurement, in situ imaging system and high-resolution CCD camera are used to capture images of deformation. We analyze images by digital image correlation technique to evaluate the in-plane finite strain components. The developed framework will aid in designing and optimizing the EAPs actuator configurations for general 3D prescribed deformation configuration.

3.2 Prestretch

Before starting any investigation of DEAs, we have to understand the important process, prestretch. Prestretch is a pre-casting process that stretch and fix the dielectric elastomer before applying electric field. From many experimental observations prestretch can significantly improve the actuation performance [21]. The improvement can be illustrated by several reasons. First of all, thinner films obtain higher Maxwell stress under the same applied voltage and are able to present larger actuation strain. The deformation of dielectric elastomer is directly driven by electrostatic forces called Maxwell stress written as Eq. 3.1, where ε_0, ε, and E stands for vacuum permittivity, relative dielectric constant, and electric field, respectively.

$$\sigma_{zz} = -\frac{1}{2}\epsilon_0\epsilon E^2 \tag{3.1}$$

According to definition, Maxwell stress, the major driving force of dielectric elastomer actuators, is proportional to the electric field, which is defined by electric potential over the DEA thickness. In other words, for the same voltage input, the thinner the DEA membrane, the higher the electric field, Maxwell stress, as well as strain. Thus, since prestretch will thinner membranes due to material incompressibility, we may obtain higher actuation strain under the same input voltage with a prestretch membrane. Second, prestretch prevents wrinkling. Wrinkle is a local instability happens on DEAs when elastomer membranes are under in-plane compression which results from excess expansion being constrained by boundaries. Therefore, by applying prestretch and keeping DE membranes under tension, compression on the tensioned membranes will become relaxation. In other words, prestretch works as buffer that is capable of digesting unwanted compression and reduces occurrence of failure. Third, prestretch postpose the occurrence of material breakdown. In previous study [30], a theory has been provided showing that prestretch postpone intersecting of electrical breakdown voltage curve and material

breakdown curve which may lead to failure. With prestretch, dielectric elastomers are able to start deforming under applied voltage without excessing the tolerance of dielectric breakdown voltage.

3.3 Material Properties

The first step of establishing a practical framework is to understand the material. In this project, 3M VHB 4910 acrylic tapes are the major material used as the dielectric elastomer. It is considered as hyperelactic material and its material properties can be perfectly described by using Ogden hyperelasticity model [35] (see Eq. 3.2) with first and second order coefficients shown in Table 1 [6].

$$\sigma_\alpha = \sum_{p=1}^{N}\left(\mu_p \lambda_p^{\alpha_p} - \mu_p \lambda_p^{-\frac{1}{2}\alpha_p}\right) \tag{3.2}$$

Coefficients		
	μ_p(kPa)	α_p
First order	92.29	1.13
Second order	0.01682	5.343

Table 1 Parameter of 3M VHB 4910 acrylic tapes described in Ogden hyperelasticity model

By applying material parameters into Eq. 3.2 and using finite element software to simulate uniaxial tensile tests, the stress-strain curves of VHB with different prestretch value are plotted in Fig. 5. In this figure, it is obvious that four curves with different prestretch almost fit into the same nonlinear curve. This implies that different values of uniaxial prestretch do not significantly affect material properties on other directions but do changes material stiffness on the prestretch direction. We can also interpret from this figure that the larger the strain is, the stiffer the VHB tape becomes.
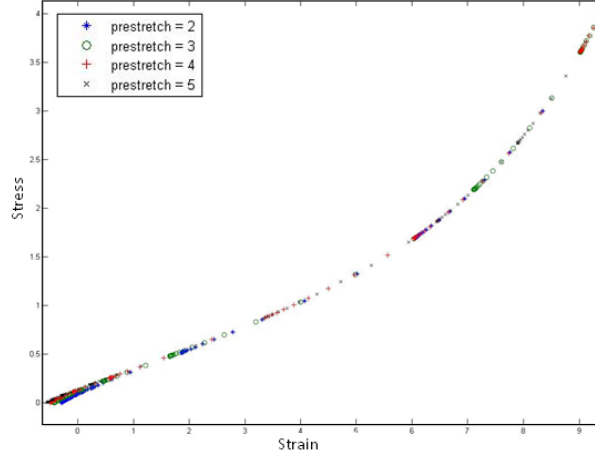
Fig. 5 Stress-strain curves of VHB with different prestretch values

That is to say, if we apply different levels of prestretch on planar DEA and then apply uniform electric filed, the actuation strain should be non-uniform and the deviation will be related to prestretch value.

The framework we use is user material subroutine with commercial finite element software, ABAQUS, provided by Dr. Wei Hong. It's Neo-Hookean based material model that couples the applied electric field to the actuator mechanical deformation. Here, we used Neo-Hookean material model instead of Ogden model for simplification. An incompressible Neo-Hookean material model under uniaxial extension is depicted with Eq. 3.3 - 3.6 where W is strain energy density, μ is the shear modulus, σ is stress, and λ is stretch.

$$\sigma_{11} - \sigma_{33} = \lambda_1 \frac{\partial W}{\partial \lambda_1} - \lambda_3 \frac{\partial W}{\partial \lambda_1} \tag{3.3}$$

$$\sigma_{22} - \sigma_{33} = \lambda_2 \frac{\partial W}{\partial \lambda_2} - \lambda_3 \frac{\partial W}{\partial \lambda_1} \tag{3.3}$$

$$W = \frac{\mu}{2}(\lambda_1^2 + \lambda_2^2 + \lambda_3^2); \quad \lambda_1 \lambda_2 \lambda_3 = 1 \tag{3.3}$$

$$\frac{\partial W}{\partial \lambda_i} = \mu \lambda_i \qquad (3.4)$$

Because of incompressibility, the poisson's ratio of the materials can be defined as 0.5 and the only modulus we need for Neo-Hookean model is shear modulus. To find a suitable modulus, we run numerical uniaxial tensile tests by using both Ogden and Neo-Hookean model. The results are plotted together for fitting and seeking the most suitable modulus value. In our concerned stretch region related to our experiments (from stretch = 2.85 to stretch = 5.7), we found that both curves are best fitted when shear modulus of Neo-Hookean model is equal to 25 kPa (see Fig. 6).

3.4 Experiments for Calibration

After developing the material materials, we attempt to run series of experiments for calibration. To prepare samples, VHB tapes were first prestretched by hand with certain value and then attached on a hollow frame with window size of 50×50 mm to fix the prestretch (see Fig. 7). The prestretch value, λ, is defined as prestretched length divided by original length, $\lambda = \frac{l}{l_0}$. In order to make hand-induced prestretch more accurate, we drawn several marks on the edge of the square to ensure they were uniformly prestretched. Carbon black was used as compliant electrodes and deposited on the VHB film in circular shape with diameter of 12.5 mm on both surfaces. An additional strip of electrode is also deposited on each side to connect to outer voltage supply (see Fig. 7).
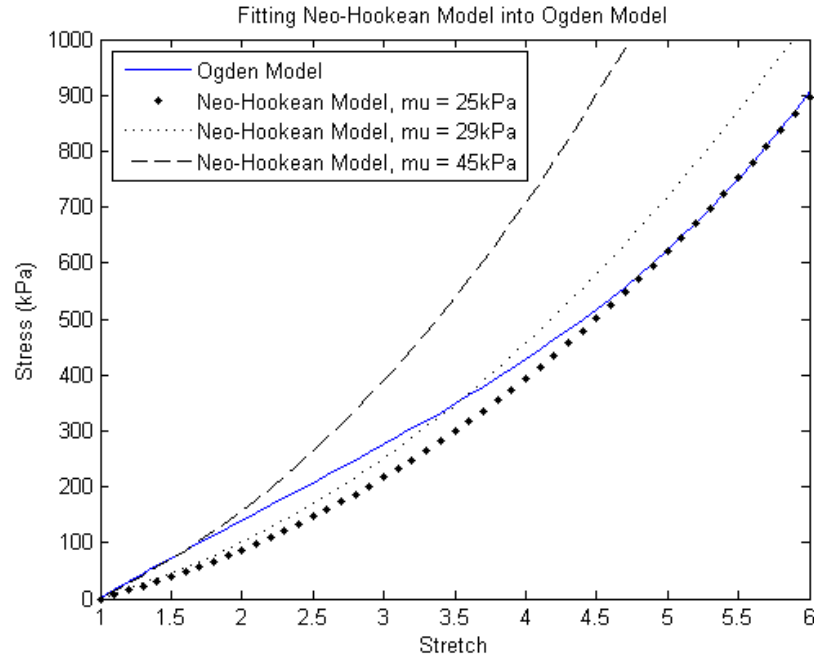
Fig. 6 Stress-stretch curve of VHB in Neo-Hookean model and Ogden model. Fitting Neo-Hookean model into Ogden model with most suitable shear modulus value.

For investigation of prestretch effect, two samples with different biaxial prestretch ratios but same total area prestretch were prepared in this project as shown in Fig. 8. Sample 1 is the equal bi-axial prestretch with stretch = 4 on both axes. Sample 2 is the unequal bi-axial prestretch with stretch = 5.7 on x-axis and stretch = 2.85 on y-axis (the prestretch ratio of two axes, $\frac{\lambda_x}{\lambda_y}$, is equal to 2). Total area stretch are remained the same on both samples to endure the thickness are the same and thickness factor would not influence the applied electric filed.

Samples were setup in situ imaging system with high resolution CCD camera (2448×2048 pixel, Grasshopper, Point Grey Inc.). Reference and deformation images were capture before and after voltage (4.8 kV) applied. We also used digital image correlation method to evaluate the in-plane finite strain components. Alumina powders were deposited on the

surfaces of samples in order to create grey scale pattern. This method offered non-contact shape and deformation measurement solutions for materials testing. Measurements could be made on length scales ranging from microns to meters and time scales as small as nanoseconds depend on captured images frames.
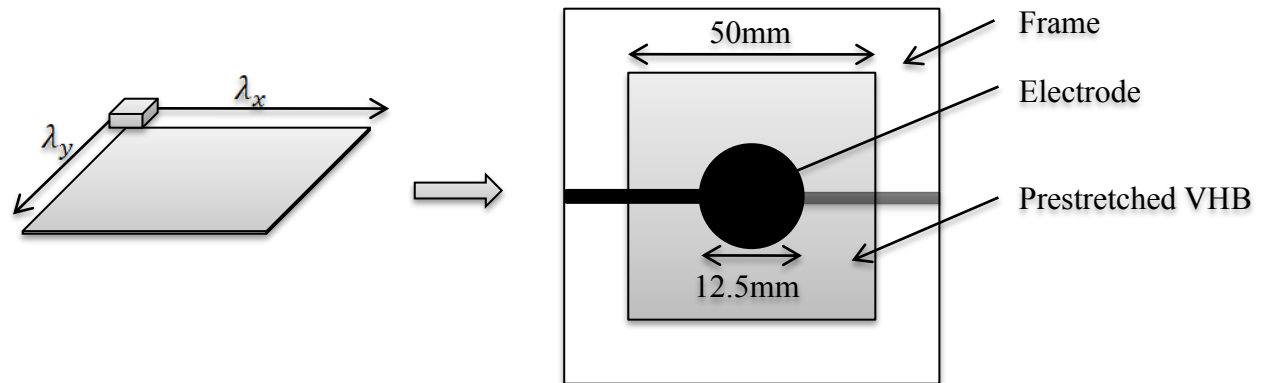
Fig. 7 Process of sample preparation.

Sample1: Equal biaxial prestretch

12.5mm
12.5mm ➜ 50×50 mm
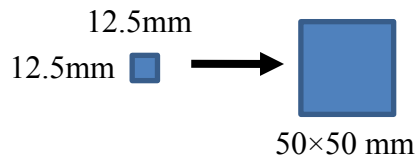
X-axial prestretch: $\lambda_x \sim 4$
Y-axial prestretch: $\lambda_y \sim 4$
Total area prestretch: 16x

Sample2: Unequal biaxial prestretch

8.75mm
17.5mm ➜ 50×50 mm
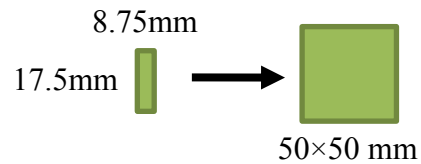
X-axial prestretch: $\lambda_x \sim 5.7$
Y-axial prestretch: $\lambda_y \sim 2.85$
Total area prestretch: ~16x

Fig. 8 Parameters of prestretch of VHB planar actuator, sample 1 and sample 2

3.5 Experimental Results

The experimentally evaluated results are shown in Fig. 9. In the figure, white circles represent the original circle size and the black regions are the active area stimulated under 4.8 kV of voltage. We can obviously observe that the circle remains its shape in equal biaxial prestretch

case (sample 1, Fig. 9a), while the circle is elongated within vertical direction in unequal biaxial prestretch case (sample 2, Fig. 9b). In addition, we have noticed that the elongated direction is the direction with less prestretch. That is to say, the direction with larger prestretch induced smaller actuation strain whereas the direction with smaller prestretch induced larger actuation strain. This result corresponding to the material nonlinearity of VHB shown in Fig. 5 that VHB tapes become stiffer under higher stretch and result in less actuation strain.

We also represent the strain field results in Fig. 10. In the figure, we can observe the distribution of strain that high strain is concentrated on the edge of intersection of active and inactive regions. Strain at the middle part of active region is very small even close to zero. Besides, for the unequal biaxial prestretch case, larger area of high strain is occurred at top and bottom region of the circle which explains why circle is elongated vertically.
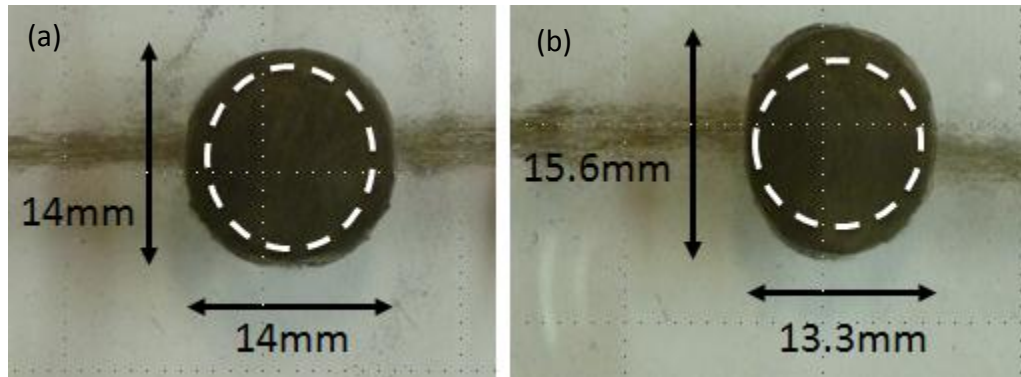
Fig. 9 Experimentally evaluated results of (a) equal biaxial prestretch and (b) unequal biaxial prestretch of planar DEAs

3.6 Comparison of Experiments and Simulation

For calibration, we compare the actuation stretch in experiments and simulation and the results are shown in Table 2. We can see that the λ results of equal biaxial prestretch case and the

λ_x results of unequal biaxial prestretch case are the very close, whereas the λ_y results of unequal biaxial prestretch case have quite obvious deviation. Reviewing stress-stretch curves shown in Fig. 6, since we choose 25 kPa as shear modulus for Neo-Hookean model, it can be observe that when λ is greater than 4, the Neo-Hookean model curve is almost perfectly fitted with Ogden model, while when λ is less than 4, there are larger difference. Therefore, this result is believed to be related to material nonlinearity that Neo-Hookean material model could not perfectly present. This deviation could be modified with other material model which is more suitable for the region of stretch level in our experiments in our future work.
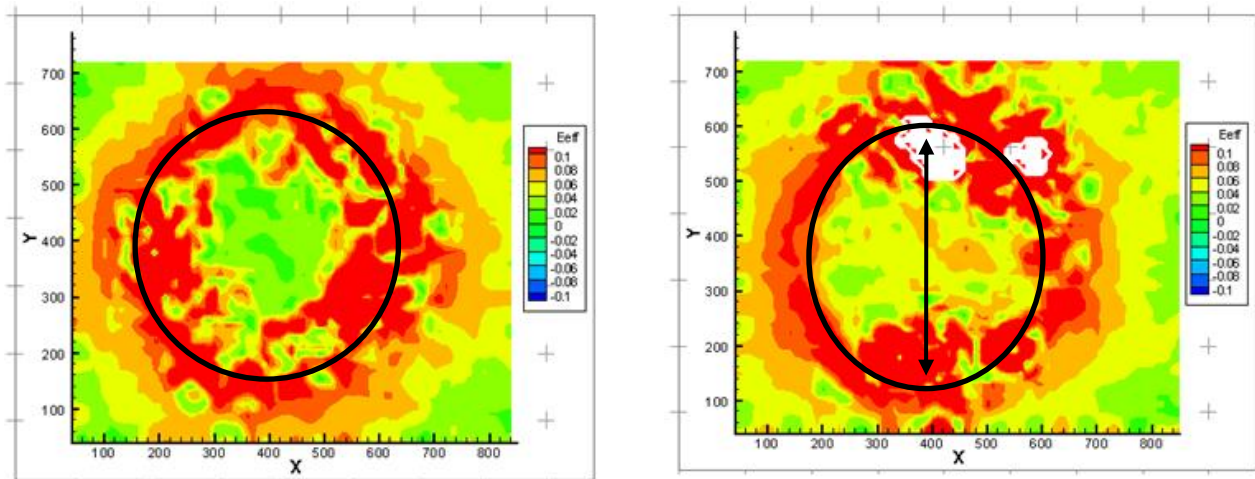
Fig. 10 Strain field results of both sample 1(left) and sample 2 (right) by using digital image correlation analysis

	Actuation stretch	Experiment	Simulation
Equal biaxial prestretch	$\lambda_x = \lambda_y$	1.101	1.125
Unequal biaxial prestretch	λ_x	1.062	1.07
	λ_y	1.25	1.14

Table 2 Actuation stretch in experiment and simulation

3.7 Conclusions

To sum up this work, we have clear understood of the mechanism of dielectric elastomer actuators and set up a practical framework. We present material nonlinear mechanical response of VHB on planar DEA and with different configuration of prestretch with different biaxial stretch ratios. Finite strain components in deformation course are provided by using images were analyzed by digital image correlation technique. The measurements are also used to calibrate a Neo-Hookean based material model built into a user-material subroutine with the ABAQUS commercial finite element package that couples the applied electric field to the actuator mechanical deformation. The simulation results are close to experimental observation with little deviation occurred in lower prestretch cases. The results show that prestretch will influence actuation strain where the direction with higher prestretch tends to have lower actuation, whereas the direction with lower prestretch tends to have higher actuation strain. The established framework can be used later for development of more complex DEAs.

Chapter 4. Fabrication and Analysis of New Dielectric Elastomer Actuator Design

4.1 General introduction

In recent studies, DEAs performance has been shown to have great improvement by introducing prestretch [20]. Concurrently, prestretch also reduced the total actuation strain from the maximum strain that materials are able to bare. Besides, prestretch process has several additional operational setbacks. For example, weight and space that the prestretch-support structures provide are much more than dielectric elastomer itself [14] [19]. In addition, non-uniform prestretch and stress relaxation may affect subsequent actuation as shown in previous section and cause local strain division. From our previous experimental observation of planar DEAs (see chapter 3), actuation strain of DEAs is controlled by the biaxial prestretch ratio. Direction with larger prestretch tends to induce lower actuation strain, and, vice versa, direction with lower prestretch tends induce higher actuation strain. Besides, since our ultimate goal is developing soft actuators which can imitate octopus arm, we cannot have actuators with firm frames included. Therefore, one of our goals in this work is to develop a method of fabricating freestanding DEAs without the support of firm frames and the need of membrane prestretch.

Aside from the structural effects of prestretch, the resulting membrane thickness reduction enhances the actuation performance. Theoretically, thinner films obtain higher Maxwell stress under the same applied voltage and are able to present larger actuation strain. According to definition (see Eq. 3.1), Maxwell stress, the major driving force of dielectric elastomer actuators, is proportional to the electric field, which is defined by electric potential over the DEA thickness. That is to say, for the same voltage input, the thinner the DEA membrane, the higher the electric field, Maxwell stress, as well as strain. Thus, to forgo the

prestretch process and build up freestanding actuators, a much thinner DE membranes have to be utilized. Much thinner DEA membranes are highly impractical for assembly and energy densities.

It has been shown that stacking planar expanding actuator and inactive layer together can induce bending and non-planar movement [14]. Expanding on the bi-material laminate principles, we provided a different method of constructing active/ inactive-layer combined structure that demonstrated more complicated 3-dimensional deformations. Our strategy was to manufacture laminates of dielectric elastomers with geometrically confining reinforcement to enable complex out-of-plane deformation without the need of prestretch. The stiffeners cover small area of the surface of the planar actuators instead of full-area of the inactive layers. These stiffeners will constrain the planar expansion deformation along their axes, inducing a thickness gradient of the expansion with thin the DEAs laminates. As a result, a local curvature of the entire assembly will be induced. In other words, these stiffeners guided the active membrane deformation to form the targeted 3D complex shapes.

In this study, we fabricated one dimensional test structures to analyze and understand the general material and geometric parameters on the induced deformation characteristics and the corresponding role of curvature. Analytical models of the deformation pattern are developed for further integration into the control algorithm. Furthermore, we fabricated test structures with different configuration of stiffeners to generate 3D configurations. For complex geometries and stiffeners, finite element to optimize the structure for given prescribed deformation pattern.

4.2 Materials Selection

Several dielectric elastomers and along with compliant electrodes have suggested in literatures [3] [5] [16]. Here, in addition to acceptable performance and geometric requirements

for our unique shell-like actuator, we are also focused on availability of materials and ease of manipulation and prototype assembly of different flexible actuator configurations.

A. Dielectric elastomer

A dielectric elastomer: 3M VHB (F9460PC) transfer tape was chosen in this study due to their suitable electro-mechanical properties of the tape core material, and the outer adhesive features. The 3M VHB tapes has been utilized in many DEAs prototypes [1] [3] [21], due to their high dielectric constant (4.7), high compliancy (~ 0.1 MPa), and great ability to withstand very large axial stretch up to 6 times [6] [7]. Furthermore, F9460PC tapes are ultrathin film with thickness of only 50 μm, which is thinner than VHB 4910 tapes after 4 times of biaxial prestretch. This geometry feature pretty much satisfies the requirement of thin DE membrane in our actuator design. Besides, benefiting from their adhesive surface, it is easy to deposit compliant electrodes even in powder form. The adhesive surface enables multiple stacking of fabricated unit cells for multi-layer structures.

B. Compliant electrodes

For compliant electrodes, carbon black powder (Super C65, TIMCAL Inc., USA) was chosen in this study. In general, carbon-based powders (alone or suspended in oil or grease) are very good compliant electrode candidates for DEAs. They have outstanding electrical conductivity while providing great compliance and tolerance to large strains. Carbon black is selected in this study due to: (i) ease of handling compared to grease, (ii) better packing (percolation) and uniform area coverage, especially during actuation. We noticed that graphite, powder with flake-like structure forms discontinuous electrode especially upon activation, and thereby limits the performance. (iii) Carbon grease (Carbon conductive grease, MG Chemicals Inc., USA) tends to remain viscous after application, making it prone for smearing and short

circuits; whereas powder is always dry and will not be spread around. And (iv) carbon grease gets to squeeze out during the fabrication of multi-layer structure. Also, since it remains in the viscous form, the ease of sliding increases the difficulty of peeling off back paper of a VHB tape that is adhered on another layer with electrodes in between.

C. Stiffener

For stiffener, 3M Scotch Magic tapes (~56 μm thick) were chosen in this study. The purpose of using stiffeners is to create an inactive layer that will not expand but can bend during actuation. Thus, an intermediate stiffness and thin sections that allow bending but no expansion should be the major and necessary criteria of material selection. 3M Magic scotch tapes not only fulfill the requirement but also have very good availability which is excellent for prototyping fabrication and demonstration.

4.3 Fabrication Procedure

The manufactured device has a square shape of 25×25 mm. It contained an active area in the middle with 22×22 mm and inactive area of 1.5 mm around the edge for sealing and preventing circuit shorting (see Fig. 11a). To construct a DEA sample, first, cut a piece of 25 mm wide VHB F9460PC tape. A window mask of 22×22 mm opening is attached to the VHB tape. The cut-out area was placed at the center of the tape. Carbon black powder was uniformly deposited on VHB film by brushing within the square pattern on the non-adhesive sheet. From experiences, we noticed that local non-uniform electrodes would increase the possibility of failure. It was not only due to defects easily forming at these non-uniform areas while manufacturing multi-layer structures, but also due to circuit shorting induced by local variation of the applied electric field. Therefore, we covered the sample up with another non-adhesive

sheet, slightly press and smear the depositing area. This step would make carbon black particle completely attached on VHB tapes uniformly with homogenous thickness and particle amount. Next, a long-narrow shape of aluminum foil was attached at the edge of sample surface slightly touching the area with carbon black which was used as attachment electrodes. Finally, covered the sample up with another VHB F9460PC tape and finish 1-stack construction. We repeated the process described above with alternating the attaching position of alumina foil to separate positive and negative electrode and fabricate multi-layer structure. As an example, a sketch of a 2-stack structure (which is the minimum stack of basic DEA design) is shown in Fig. 12a, and 3-stack structure is shown in Fig. 12b.

For the stiffener part, 3M Magic scotch tapes were cut into long-narrow shape with width of 2 mm. Two configurations of stiffener reinforcement were applied in this study for analyze as shown in Fig. 11b and c.

4.4 Experiments

In the experiments, DEA samples were hung from the attachment electrodes and connected to the high voltage circuit terminal [1] . The applied step voltages ranged from 2 to 3.2kV. A DC-DC converter (Q-80, EMCO Inc.) is utilized. The converter has a high DC voltage amplifier linear range of 0 – 8kV output for 0–5V input. The actuator movements were captured by high-resolution CCD camera (2448×2048 pixel, Grasshopper, Point Grey Inc.) for curvature analysis.
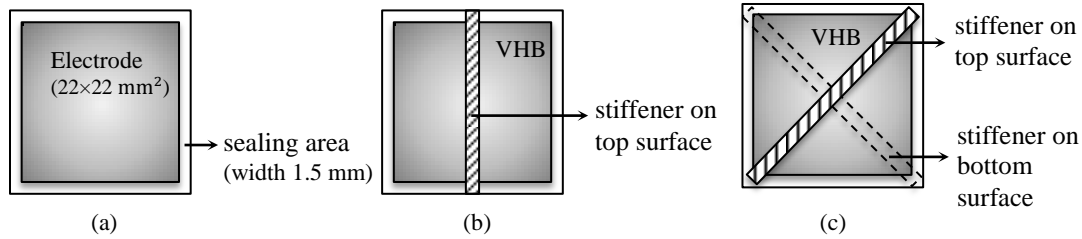
Fig. 11 Sketches of DEA samples. (a) Top view of unit-cell DEA structure and its measurement with (b) Strip configuration reinforcement attached, and (c) Cross configuration reinforcement attached.
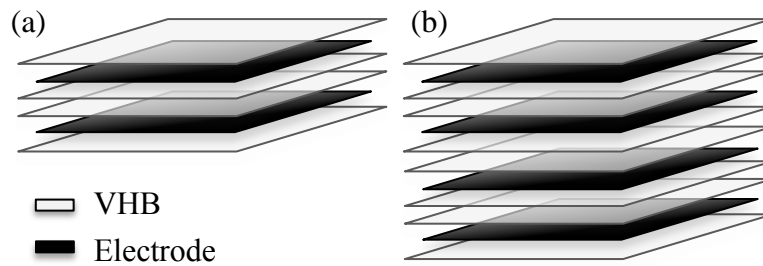
Fig. 12 Sketches of DEA samples fabrication with side view of different stack configurations: (a) 2-stack and (b) 3-stack.

4.5 Results

In this section, we will first discuss the case of strip configuration. Bending curvatures were calculated from the recorded images under different activation voltage, and for different stack configuration. Also, curvatures were also calculated analytically and numerically for comparison. Besides, the energy efficiency is also calculated and presented. Next, we further use the experimental results for the simple rotational degree of freedom configuration to calibrate the FEM model. The model is used to analyses the other complex deformation patterns.

A. Strip configuration

The experimentally evaluated bending curvatures under different level of applied voltage are shown in Fig. 13. The curvature of the entire actuator is assumed to be approximately uniform for ease of numerical analysis. Measurements were conforming to the active region only and the result of curvature is shown in Fig. 15. In order to capture clear bending motions without random surface buckling, piece of transparency papers were attached at the bottom edge. The experimental results show that the stack curvature increases with the stack number of active layers. Such trend in active materials is different than the behavior of simple beam bending, wherein thicker beam would bend less under the same applied load.
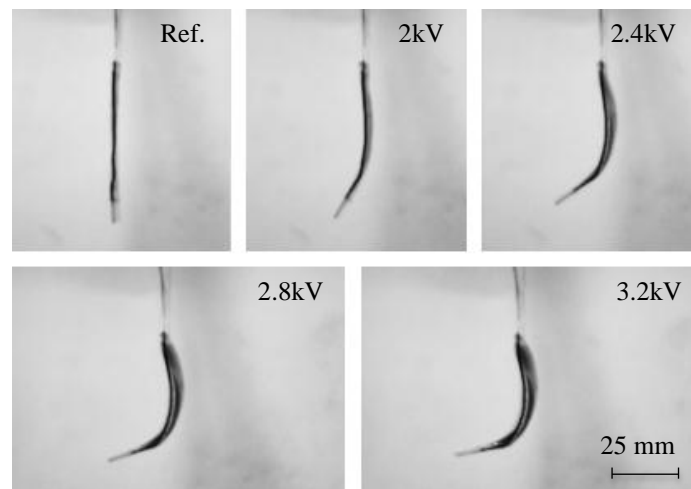
Fig. 13 Deformation sequence (0-3.2kV) of 4-stack configuration

The increase of the number of active stacks in the actuator configuration would increase the driving forces that have to remain in balance with the forces generated within the stiffening layer. Moreover the role of the inactive cover layer on each side of the stack has to be considered. In our design, we had samples covered with an additional VHB layer on each of the top and

bottom surfaces for protection of the electrodes (Fig. 11a and b). As a result, the more stacks we have, the less effect we would get from them as they were being diluted.

To understand this trend, we utilized the Timoshenko's analysis of bi-metal thermostats [29] and introducing the Maxwell stress instead of the thermal effect to arrive at the general deformation representation under applied electric field. In Timoshenko's analysis, we can first simply draw the free-body diagram as in Fig. 14. In the diagram and following equations, q and m are shear force and moment on the interface, Q and M are the concentrated axial force and moment on each layer, ε represents strain of in-plane expansion induced by Maxwell stress, E is stiffness, h is thickness, A is cross-section area, I is the section second moment of area, and subscribes s and a represent stiffener and DEA layer respectively. Through the diagram, horizontal and vertical displacement of layer 1 and layer 2 can be easily written in Eq. 4.1 - 4.4. Due to the compatibility of displacements along the interface, $u_1(x)$ and $u_2(x)$ are required to be equal, and so do $v_1(x)$ and $v_2(x)$. Therefore, q and m can be solved in Eq. 4.5 and 4.6.
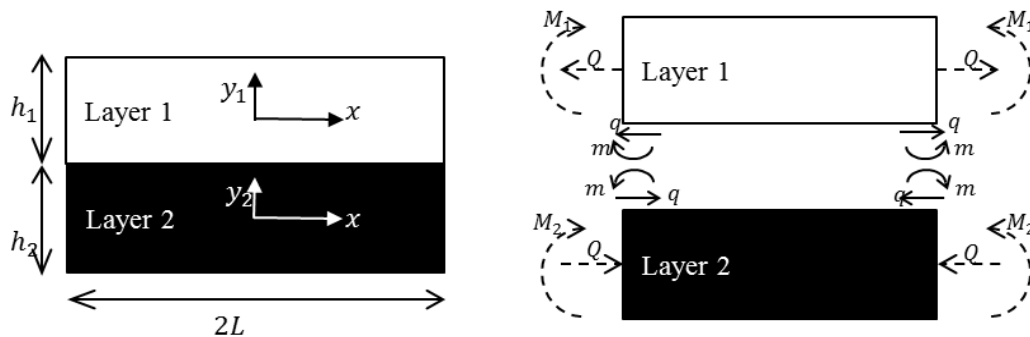

Fig. 14 Free-body diagram of bi-layer structure

Layer 1 (DEA layer)

$$u_1(x) = \varepsilon_1 - \frac{qx}{E_1 A_1} - \left(\frac{qh_1}{2} - m\right)\frac{x}{E_1 I_1}\frac{h_1}{2} \tag{4.1}$$

$$v_1(x) = \left(\frac{qh_1}{2} - m\right)\frac{x^2}{2E_1 I_1} \tag{4.2}$$

Layer 2 (stiffener layer)

$$u_2(x) = \varepsilon_2 + \frac{qx}{E_2 A_2} + \left(\frac{qh_2}{2} + m\right)\frac{x}{E_2 I_2}\frac{h_2}{2} \tag{4.3}$$

$$v_2(x) = \left(\frac{qh_2}{2} - m\right)\frac{x^2}{2E_2 I_2} \tag{4.4}$$

$$q = \frac{\varepsilon_1 - \varepsilon_2}{\frac{1}{E_1 A_1} + \frac{1}{E_2 A_2} + \frac{(h_1 + h_2)^2}{4(E_1 I_1 + E_2 I_2)}} \tag{4.5}$$

$$m = \frac{\varepsilon_1 - \varepsilon_2}{2\left[\frac{1}{E_1 A_1} + \frac{1}{E_2 A_2} + \frac{(h_1 + h_2)^2}{4(E_2 I_2 + E_1 I_1)}\right]} \frac{h_1 E_2 I_2 + h_2 E_1 I_1}{E_1 I_1 + E_2 I_2} \tag{4.6}$$

The relation of q, m and Q, M can be written in Eq. 4.7. In addition, the total stress of each layer can be obtained from summing axial stress produced by Q and bending stress produced by M (see Eq. 4.8 and 4.9).

$$Q = q, \qquad M_1 = \frac{qh_1}{2} - m, \qquad M_2 = \frac{qh_2}{2} + m \tag{4.7}$$

$$\sigma_{xx}|_1 = \frac{-Q}{A_1} - \frac{M_1 y_1}{I_1} \tag{4.8}$$

$$\sigma_{xx}|_2 = \frac{Q}{A_2} - \frac{M_2 y_2}{I_2} \tag{4.9}$$

In the first step, the effective deformations of active and inactive DE layers are considered. Since a symmetric lay-up is considered here, only axial deformation will commence. The cover layer would reduce the resulting strain by a linear factor, β, for all activation voltage

(1/2, 2/3, 3/4, for the 2, 3, and 4-stacks respectively). Second, the role of the stiffener (including geometry and material property) is considered. Employing Eq. 4.5 and 4.6 into Eq. 4.2 or 4.4, an explicit expression of the membrane vertical displacement can be obtained as a function of the effective Maxwell stress induced strain and the membrane geometry shown in Eq. 4.10.

$$v(x) = \frac{\text{effective Maxwell stress induced strain}}{4\left[\frac{1}{E_1 A_1} + \frac{1}{E_2 A_2} + \frac{(h_1 + h_2)^2}{4(E_1 I_1 + E_2 I_2)}\right]} \frac{h_1 + h_2}{E_1 I_1 + E_2 I_2} \tag{4.10}$$

Rewriting the effective Maxwell stress induced strain as a function of the applied voltage potential, the membrane vertical deflection (membrane edge relative to center) is given by Eq. 4.11. Here, v is poisson's ratio, ϵ_0 is vacuum permittivity, ϵ is relative dielectric constant, V is applied voltage potential and d is thickness of active region of DEA.

$$v(x) = \frac{\frac{1}{E_2}\left[v \frac{1}{2}\epsilon_0 \epsilon \left(\frac{V}{d}\right)^2\right] \times \beta}{4\left[\frac{1}{E_1 A_1} + \frac{1}{E_2 A_2} + \frac{(h_1 + h_2)^2}{4(E_1 I_1 + E_2 I_2)}\right]} \frac{h_1 + h_2}{E_1 I_1 + E_2 I_2} \tag{4.10}$$

Accordingly, the membrane curvature, κ, is given by Eq.4.11 which is plotted in Fig. 15.

$$\kappa = \frac{1}{Radius} = \frac{|2v|}{L^2 + v^2} \tag{4.11}$$

The analytical results concur with the experimentally measured trends. Deviation at higher voltages arises from large deformation material non-linearity, an issue that would be addressed in the numerical framework.

In above equations, a linearized material constitutive relation is assumed to account for the Maxwell stress induced planar expansion. Nonlinear material models are considered within the FEM framework.

Equation 4.10 shows the competing role of the stiffener material and geometry on the performance of the DEA. It can be used to screen different stiffness materials and actuators for the optimization of the required force and stroke characteristics.

Furthermore, we attempt to calculate energy efficiency of the electrical input energy and the mechanical output energy. Energy efficiency, η, is calculated from the stored elastic strain energy divided by the input electric energy, as depicted Eq. 4.11. Here, σ is the in-plane axial stress, E_y is the stiffness, C is the total capacitance, and V is the applied voltage. We get the highest efficiency, η, equals 2.5% at 3-stack configuration under input voltage of 3.2kV.

$$\eta = \frac{U_{\text{elastic}}}{U_{\text{electric}}} = \frac{\frac{length \times width}{2E_y}\int \sigma^2 dy}{\frac{1}{2}CV^2} \tag{4.11}$$

B. Cross configuration

Based on the understating of bending induced by strip configuration of stiffeners, we attempted to study more complicated configuration of reinforcements. By using commercial software, ABAQUS, of finite element method analysis with user material discussed in chapter 3, we coupled the applied electric field to the resulting deformation. The images capture from experiments and simulations are shown in Fig. 16. Fig. 16a and b are the sketch and experimental results of saddle-shape deformation of DEA after applying voltage with cross-configuration of stiffener reinforced (see Fig. 16c). Fig. 16c is the deformation of quarter of DEA in FEM analysis.

4.6 Conclusions

In this work, we presented a new design for a dielectric elastomer actuator (DEA) with geometrically confining reinforcements. The main contribution is that these reinforcements

induced complex 3-dimentional motions without the need of the DEA prestretch. We started the study with strip-stiffener reinforcements with different stack configurations which presented a fundamentally new bending mechanism. We used in situ imaging system to capture the pattern of complex deformation to evaluate the surface curvatures. The results were analyzed analytically using the bi-laminate theory that showed an increase of the number of active stacks in the actuator configuration would increase the driving forces that have to remain in balance with the forces generated within the stiffening layer. After this, the energy efficiency between stored elastic strain energy and input electric energy was calculated as well.

In addition, a finite element material model discussed in section 3 is also developed to couple the applied electric field to the resulting deformation for analyzing the more complex deformation patterns such as the complex saddle-shape we presented in this work, This work will lead to the development of flexible continuous robotics, utilizing combination of the proposed deformation mechanisms, thereby enabling many controllable degrees-of-freedom.
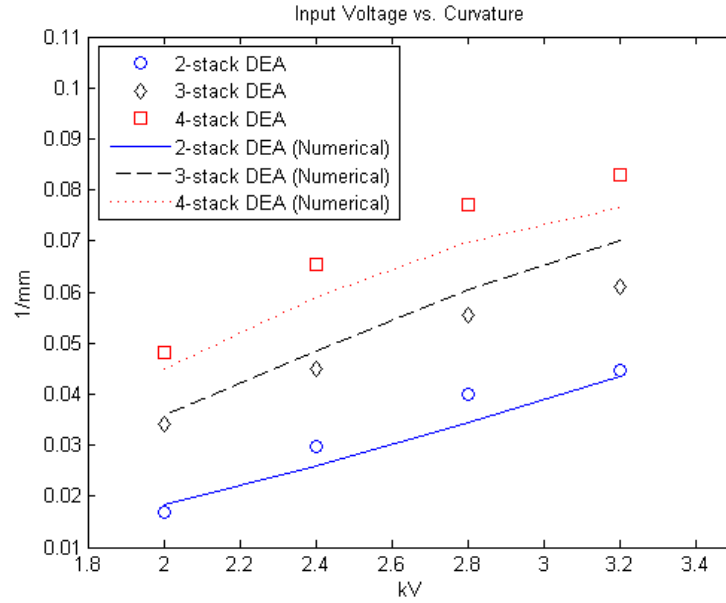
Fig. 15 Experimental and numerical results of actuation curvature of DEAs with different stack configurations under different applied voltage
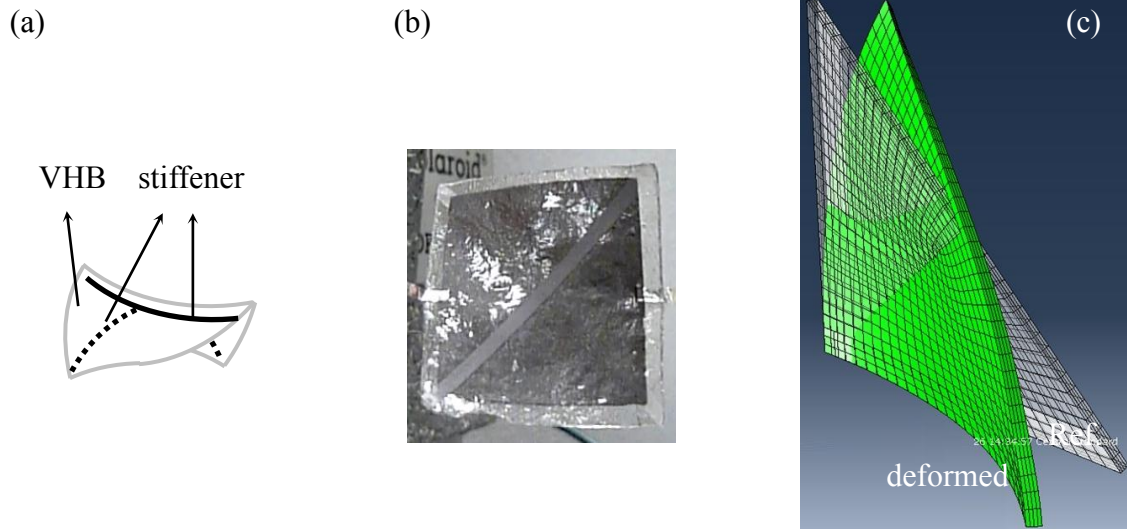

Fig. 16 (a) Sketch, (b) experimental, and (c) FEM results of saddle-shape deformation of DEA with cross configuration reinforcements.

Chapter 5. Conclusion and Future Work

5.1 Conclusion

Electroactive polymers have been proposed for one of the suitable materials for compliant and lightweight biomimic actuators performing as artificial muscles. To develop a practical biomimic actuator with good performance, we started from understanding material properties and developing practical framework. In literatures, we obtained the knowledge of the fundamental working mechanism, its nonlinear material properties, and how a pre-casting process, prestretch, influence the performance. Therefore, our first objective was to choose a suitable material constitutive model for framework development that satisfied the material properties. A Neo-Hookean material based model built into a user-material subroutine with the ABAQUS commercial finite element package provided by Dr. Hong that couples the applied electric field to the actuator mechanical deformation was used in this study. To calibrate the model, we carried out a series of experiments. We fabricated planar DEAs with inducing different equal/ unequal biaxial stretch ratios on VHB membranes and test their actuation strain under applied electric field. Circle shape of active regions were deposited on each sample in order to see any shape change caused by material nonlinearity effects. We not only measured general shape change of active area but also analyzed the in-plane finite strain components during the course of deformation. High resolution images of the deformed state were captured in situ captured system in order to evaluate in-plane strain field by digital image correlation technique. The in-plane results showed that for a planar DEA, the direction with higher prestretch tends to have lower actuation, whereas the direction with lower prestretch tends to have higher actuation strain. This result corresponds to our understanding of material nonlinearity of VHB in stress-strain curve that VHB becomes stiffer when it is under higher

stretch. We figured our model had corresponding trend of results to experiments mostly except small deviation in the case of VHB membranes under smaller prestretch. We consider it was due to that in the prestretch level in our experiments, Neo-Hookean model could not 100% fit with VHB stress-strain relation in reality. This could be improved by modifying the model by changing suitable modulus or other material models for the specific target level of prestretch.

After understanding more about the material and building a practical framework, we were focusing on fabrication of new design of DEAs. Our ultimate goal is developing soft actuators suitable for artificial muscle applications. Therefore, we have to surmount frame-requirement problems existing in DEAs nowadays. In this study, we presented a new concept of freestanding DEAs with no prestretch requirement. This kind of DEA is fabricated in thin multi-layer structure with geometrically confining reinforcements that were capable of inducing complex 3-dimentional motion. To analyze our prototyping actuators, first, different stack configurations with simple strip configuration of reinforcement were fabricated for bending analysis. The results were investigated analytically using the bi-laminate theory that showed an increase of the number of active stacks in the actuator configuration would increase the driving forces that have to remain in balance with the forces generated within the stiffening layer. Also, the energy efficiency between stored elastic strain energy and input electric energy was calculated as well. After this, more complex configuration of reinforcements were fabricated and presented in experiments and simulation. Here we used the Neo-Hookean material based model we calibrated in prior part of work operating in commercial finite element software (ABAQUS) to present the numerical result of motion.

5.2 Future Work

After having fabricated and analyzed a unit-cell of soft actuator, our next step is to try different configurations of stiffener on unit-cell of DEA and investigate more complicated deformation. We are also looking to try to construct numbers of unit-cell for higher degree-of-freedom DEAs with and electrical control system. In the meantime, the framework we established will be a very useful tool for developing future practical DEAs that may ultimately imitate the complex motion in Mother Nature.

References

[1] A. Wingert, Matthew D. Lichter, and Steven Dubowsky, Fellow IEEE. "On the Design of Large Degree-of-Freedom Digital Mechatronic Devices Based on Bistable Dielectric Elastomer Actuators." IEEE/ASME transactions on mechatronics, Aug. 2006: vol. 11, no. 4,.

[2] Bar-Cohen, Y. Ed., Electroactive, Polymer (EAP) Actuators as Artificial Muscle, 2nd edition. Bellingham, WA: SPIE Press, 2004.

[3] F. Carpi, P. Chiarelli, A. Mazzoldi, and D. De Rossi. "Electromechanical characterisation of dielectric elastomer planar actuators: comparative evaluation of different electrode materials and different counterloads." Sensors & Actuators: A. Physical, 2003: 107(1):85–95.

[4] F. Carpi, P. Chiarelli, A. Mazzoldi, and D. De Rossi. "Folding dielectric elastomer actuators." Smart Materials and Structures, 2007: Vol.16, 300-305.

[5] G. Gallone, F. Galantini, and F. Carpi. "Perspectives for new dielectric elastomers with improved electromechanical actuation performance: Composites versus blends." Polymer International, 2010: 59(3):400–406.

[6] G. Kofod. "The static actuation of dielectric elastomer actuators: how does pre-stretch improve actuation?" JOURNAL OF PHYSICS D: APPLIED PHYSICS, 2008.

[7] G. Kofod,. Dielectric elastomer actuators, Ph.D. thesis. The Technical University of Denmark, Sept. 2001.

[8] G. Kofod, M. Paajanen, S. Bauer. "Self-organized minimun-energy structures for dielectric elastomer actuators." Applied Physics A, 2006: Vol.85, 141-143.

[9] G. Kovas, L. During, S. Michel, G. Terrasi. "Stacked dielectric elastomer actuator for tensile force transmission." Sensors and Actuators A: Physical, 2009: Vol. 155, 299-307.

[10] I. Hunter, S. Lafontaine. "Actuators Workshop." Tech. Dig. IEEE Solid State Sens., 1992: 178.

[11] K. J. Kim, M. shahinpoor. "Development of three dimensional ionic polymer-metal composites ad artificial muscles." Synthetic Metals, 2002: 78:339-353.

[12] K. J. Kim, S. Tadokoro. Eds., Electroactive Polymers for Robotic Applications: Artificial Muscles and Sensors. London, UK: Springer, 2007.

[13] K. Oguro, Y. Kawami, H. Takenaka. Osaka: Garvernment Industrial Research Institute, 1992.

[14] Kornbluh R, Perine R, Pei Q, Heydt R, Stanford S, Oh S and Eckerle J. "Electroelastomer: application of dielectric elastomer transducers for actuation, generation and smart structures." Proc. SPIE Int. Soc. Opt. Eng. 4698, 2002: 254–70.

[15] Lochmatter Patrick, Kovacs Gabor, Michel Silvain. "Characterization of dielectric elastomer actuators based on a hyperelastic film model." Sensers and Actuators A: Physical, 2007: Vol. 135, 748-757.

[16] M.Y. Benslimane, H.E. Kiil, and M.J. Tryson. "Dielectric electroactive polymer push actuators: performance and challenges." Polymer International, 2010: 59(3):415–412.

[17] Madden J D W, N. A. Vandesteeg, P. A. Anquetil, P. G. Madden, A. Takshi, R. Z. Pytel, S. R. Lafontaine, P. A. Wieringa, W. Hunter. "Artificial muscle technology: physical principles and naval prospects." IEEE J. Ocean. Eng. 29, 2004: 706-28.

[18] P Lochmatter, G Kovacs, P Ermanni. "Design and Characterization of shell-like actuators based on soft dielectric eletricactive polymers." Smart Materials and Structures, 2007: Vol. 16, 1415-1422.

[19] Pei Q, Rosenthal M, Stanford S, Prahlad H and Pelrine R. "Multiple-degrees-of-freedom electroelastomer roll actuators." Smart Mater. Struct., 2004: 13 N86–92.

[20] Pelrine R, Kornbluh R, Pei Q and Joseph J. "High-speed electrically actuated elastomers with strain greater than 100%." Science, 2000: 287 836–9.

[21] Pelrine R, Kornbluh R, Pei Q. "High-performance acrylic and silicone elastomers." Chap. chapter 4 in Dielectric elastomers as electromechanical transducers: Fundamentals, materials, devices, models and applications of an emerging electroactive polymer technology, by D. De Rossi, R. Kornbluh, R. Pelrine, and P. Sommer-Larsen, editors F. Carpi. Elsevier, 2008.

[22] R. H. Baughman, L. W. Shacklette, R. L. Elsebaumer, E. J. Electronics. "Topics in Molecular Organization and Engineering: Molecular Electronics." Kluwer, Dordrecht, 1990.

[23] R. Kornbluh, R. Pelrine, and Q. Pei. Dielectric elastomer produces strain of 380%. EAP Newsletter, 2(2):10–11, 2002.

[24] R. Pelrine, R. Kornbluh, J. Joseph, R. Heydt, Q. Pei, and S. Chiba. "High-field deformation of elastomeric dielectrics for actuators." Materials Science & Engineering C, 2000: 11(2):89–100.

[25] Roentgen, W. C. "About the Changes in Shape and Volume of Dielectrics Caused by Electricity." Annual Physics and Chemistry Series, 1880: Vol. 11, sec III.

[26] S, Ashley. "Artificial muscles." Scientific American, October 2003: pp. 52–9.

[27] Sommer-Larsen P, Kofod G, Shridhar M H, Benslimane M and Gravesen P. "Performance of dielectric elastomer actuators and materials." Proc. SPIE Int. Soc. Opt. Eng.4695, 2002: 158–66.

[28] Stella, W. Kier and M.P. "The Arrangement and Function of Octopus Arm Musculature and Connective Tissue." Journal of Morphology, 2007: 268: 831–843.

[29] Timoshenko, S. "Analysis of Bi-Metal Thermostats." Journal of the Optical Society of America, 1925: Vol. 11, pp. 233-25.

[30] X. Zhao, Z. Suo. "Theory of dielectric elastomers capable of giant deformation of actuation." Physical Review Letters, 2010: 104, 178302.

[31] Y. Yekutieli, G. Sumbre, T. Flash, and B. Hochner. "How to move with no rigid skeleton? The octopus has the answers." Biologist, 2002: 49(6):250-254.

[32] R. Perline, R D. Kornbluh, J P. Joseph, "Electrostriction of polymer dielectrics with compliant electrodes as a mean of actuation", Seneros and Actuators A: physical, 1998: 77-85

[33] W. Kier and M.P. Stella, 2007, "The Arrangement and Function of Octopus Arm Musculature and Connective Tissue," Journal of Morphology, 268:831–843.

[34] Y. Yekutieli, G. Sumbre, T. Flash, and B. Hochner, 2002, "How to move with no rigid skeleton? The octopus has the answers," Biologist, 49(6):250-254

[35] Lochmatter Patrick, Kovacs Gabor, Michel Silvain, "Characterization of dielectric elastomer actuators based on a hyperelastic film model", Sensors and Actuators A, 2007: 135: 748–757

Acknowledgments

First, I would like to thank my advisor Dr. Ashraf Bastawrows for his patience, guidance, and encouragement. His passion for science stimulates my desire of learning. He always lets me use my creativity and imagination as much as I can, and bring me back on the trail every time I get lost.

I would also like to thank my committee, Dr. Wei Hong, for his help of various finite element questions and the coding of UMAT. In addition, his knowledge of soft materials and many great ideas help me a lot with this work.

Besides, I would like to thank my other committee, Dr. Rudolphi, for introducing the beauty of computational science and the wonderful class of finite element method.

Also, I want to thank my family and friends support me every single moment while I'm studying abroad.